Title

Ca2+-activated K+ channels modulate microglia affecting motor neuron survival in hSOD1G93A mice.

Authors

Cocozza, Germana
di Castro, Maria
Carbonari, Laura
et al.

Publication Date

2018-10-01

DOI

10.1016/j.bbi.2018.07.002

Peer reviewed

HHS Public Access

Author manuscript

Brain Behav Immun. Author manuscript; available in PMC 2019 October 01.

Published in final edited form as:

Brain Behav Immun. 2018 October ; 73: 584–595. doi:10.1016/j.bbi.2018.07.002.

Ca^{2+}-activated K^+ channels modulate microglia affecting motor neuron survival in $hSOD1^{G93A}$ mice

Germana Cocozza[a,b], **Maria Amalia di Castro**[a], **Laura Carbonari**[a], **Alfonso Grimaldi**[b], **Fabrizio Antonangeli**[c], **Stefano Garofalo**[d], **Alessandra Porzia**[e], **Michele Madonna**[e], **Fabrizio Mainiero**[f], **Angela Santoni**[c,e], **Francesca Grassi**[a], **Heike Wulff**[g], **Giuseppina D'Alessandro**[e,*], and **Cristina Limatola**[*,d,e]

[a]Department of Physiology and Pharmacology, Sapienza University, Rome, Italy

[b]Center for Life Nanoscience – Istituto Italiano di Tecnologia@Sapienza, Rome, Italy

[c]Department of Molecular Medicine, Sapienza University, Laboratory affiliated to Istituto Pasteur Italia – Fondazione Cenci Bolognetti, Rome, Italy

[d]Department of Physiology and Pharmacology, Sapienza University, Laboratory affiliated to Istituto Pasteur Italia – Fondazione Cenci Bolognetti, Rome, Italy

[e]IRCCS Neuromed, Pozzilli, IS, Italy

[f]Department of Experimental Medicine, Sapienza University, Rome, Italy

[g]Department of Pharmacology, University of California Davis, Davis, CA 95616, USA

Abstract

Recent studies described a critical role for microglia in amyotrophic lateral sclerosis (ALS), where these CNS-resident immune cells participate in the establishment of an inflammatory microenvironment that contributes to motor neuron degeneration. Understanding the mechanisms leading to microglia activation in ALS could help to identify specific molecular pathways which could be targeted to reduce or delay motor neuron degeneration and muscle paralysis in patients. The intermediate-conductance calcium-activated potassium channel KCa3.1 has been reported to modulate the "pro-inflammatory" phenotype of microglia in different pathological conditions. We here investigated the effects of blocking KCa3.1 activity in the $hSOD1^{G93A}$ ALS mouse model, which recapitulates many features of the human disease. We report that treatment of $hSOD1^{G93A}$ mice with a selective KCa3.1 inhibitor, 1-[(2-chlorophenyl)diphenylmethyl]-1*H*-pyrazole (TRAM-34), attenuates the "pro-inflammatory" phenotype of microglia in the spinal cord, reduces motor neuron death, delays onset of muscle weakness, and increases survival. Specifically, inhibition of KCa3.1 channels slowed muscle denervation, decreased the expression of the fetal

Corresponding author: Cristina Limatola, Sapienza University, Piazzale Aldo Moro 5 - 00185, Rome, Italy, cristina.limatola@uniroma1.it.

*equally contributing authors

Competing interests: No competing interests declared.

acetylcholine receptor γ subunit and reduced neuromuscular junction damage. Taken together, these results demonstrate a key role for KCa3.1 in driving a pro-inflammatory microglia phenotype in ALS.

1. Introduction

Amyotrophic lateral sclerosis (ALS) is a multifactorial disease characterized by the progressive degeneration of motor neurons (MN) and muscle paralysis. Despite current treatments, patients survive less than 3–5 years after the initial diagnosis. Most ALS cases are sporadic (sALS), and only 5–10% have a familial origin (fALS). Among the latter, about 20% express a dominant mutant form of the Cu, Zn superoxide dismutase (SOD1) (Rothstein, 2009). Transgenic mice expressing a mutant SOD1 develop MN pathology, with muscle denervation and weakness similar to ALS patients (Fischer et al., 2004). Many evidence demonstrate that ALS is non-cell autonomous, with multiple co-players involved in disease progression (Robberecht et al, 2013). In particular, signals from both glial cells and muscles initiate and sustain MN degeneration (Boillée et al., 2006; Dobrowolny et al, 2008). Neuroinflammation is often associated with ALS (Philips et al., 2011): microglial reactivity, astrogliosis and lymphocyte infiltration are common in patients and in experimental models of the disease (Hall et al., 1998; Mantovani et al., 2009; Turner et al., 2004). Microglia carrying mutant SOD1 express pro-inflammatory genes, such as *il-1β, tnf-α* and *inos* (Philips et al., 2011; Almer et al., 1999; Henkel et al., 2004). Nevertheless, the exact contribution of neuroinflammation to the pathology of ALS is not clear, possibly acting in concert with additional factors. The knowledge of the molecular mechanisms driving the inflammatory responses, and their impact on MN, would be of great importance to develop effective therapeutic treatments. Among the possible modulators of the inflammatory response in the CNS, plasma membrane ion channels are good candidates, regulating membrane potential and intracellular signaling in T cells, B cells and innate immune cells such as macrophages and microglia (Feske et al., 2015; Zierler et al., 2016). In this work, we investigated the role of the intermediate-conductance, Ca^{2+}-activated K^+ channel KCa3.1, in shaping the activation state of microglia in a mouse model of ALS, the $hSOD1^{G93A}$ mice, which recapitulates many features of the human disease. In the CNS, KCa3.1 channels are expressed by microglial cells, where they regulate cell migration and phagocytic activity in physiological and pathological conditions such as glioma, ischemia, spinal cord injury (SCI) and Alzheimer's disease (AD) (Chen et al., 2011; Maezawa et al., 2012; Bouhy et al., 2011; D'Alessandro et al., 2013; Grimaldi et al., 2916). In some conditions (SCI), the expression of KCa3.1 is also reported on astrocytes and neurons (Bouhy et al., 2011). In AD, microglial KCa3.1 potentiate the neurotoxicity induced by oligomeric amyloid-*β* and lipopolysaccharide (LPS) treatment (Maezawa et al., 2012; Kaushal et al., 2007); while blocking KCa3.1 activity has beneficial effects in rodent models of multiple sclerosis and ischemic stroke, reducing TNF-α and IFN-γ expression in the spinal cord (Reich et a., 2005) or the infarcted area (Chen et al., 2016). The KCa3.1 inhibitor *per se* is not directly neuroprotective in the absence of microglia (Maezawa et al., 2011; D'Alessandro et al., 2016).

In the current study, we treated hSOD1^{G93A} mice with the selective KCa3.1 inhibitor TRAM-34 starting at the pre-symptomatic stage and analyzed the activation state of spinal cord microglia by measuring the expression levels of “pro“ and “anti-inflammatory” genes and cell morphology. We found that the chronic inhibition of KCa3.1 activity in hSOD1^{G93A} mice: i) restrained the pro-inflammatory phenotype of microglia; ii) increased the number of healthy MNs; iii) preserved the number of healthy neuromuscular junctions (NMJ) in the *tibialis anterior* muscle; iv) and their maturation level, as assessed by mRNA analysis of AChR γ and ε subunit expression and by current recording on isolated muscle fibres. Furthermore, TRAM-34 treatment delayed motor symptom appearance, as shown by prolonged muscle strength and motor coordination, and increased mice survival. Taken together, these data demonstrate a crucial role for microglia in modulating disease onset and progression, and provide prove-of-concept for the potential targeting of KCa3.1 to reduce ALS-associated neuroinflammation and to protect MNs from degeneration.

2. Materials and Methods

2.1 Animal model

The study was conducted in accordance with the ARRIVE guidelines (Kilkenny et al., 2010). All experiments and procedures were approved by the Italian Ministry of Health (authorization n. 78/2017-PR) in accordance with the ethical guidelines on use of animals from the EC Council Directive 2010/63/EU and from the Italian D.Leg 26/2014. All possible efforts were made to minimize animal suffering, and to reduce the number of animals used per condition by calculating the necessary sample size before performing the experiments. hSOD1(G93A) transgenic mice, which express about 20 copies of mutant human SOD1^{G93A} [B6.Cg-Tg(SOD1-G93A)1Gur/J line] were obtained from Jackson Laboratory (Bar Harbor, ME, USA) (RRID:IMSR_JAX:004435) (Charles River, Calco, Italy). B6.Cg-Tg(SOD1-G93A)1Gur/J were also maintained as hemizygotes by breeding transgenic males with wild-type C57BL/6J females from Charles River Laboratories, both maintained on C57BL/6J genetic background. Age-matched non-transgenic C57BL/6J mice were always used as control mice. Only male mice were used for the experiments to minimize gender-induced differences in motor impairment and survival (Choi et al. 2008). Transgenic mice were identified by PCR on DNA obtained from tail biopsies. Briefly, tail tips were digested (overnight, 58 °C) in a buffer containing 100mM Tris–HCl pH 8, 0.1 % SDS 20, 5mM EDTA pH8, 200mM NaCl and 20 mg/ml proteinase K (Ambion-Thermo Fisher, Germany, #2548) and the genomic DNA was amplified with SsoFast Eva Green Supermix (Bio-Rad, California, #172-5201) using the following primers: SOD1 forward 5′-CATCAGCCCTAATCCATCTGA-3′; SOD1 reverse 5′-CGCGACTAACAATCAAAGTGA-3′. Animals were housed in regular polycarbonate cages (30 × 16 × 11 cm), 2–3 per cage, at constant temperature (22 ± 1 °C) and humidity (50%), and were kept on a 12-h light cycle (light 7 a.m.to 7 p.m.). Housing comprised nesting objects, with bedding (sawdust) materials. Food (regular chow, containing 14% protein, 5% fat, 3041 kcal ME/kg) and water were freely available. Microbiological analyses were routinely (each 3–4 months) performed and defined endemic Norovirus and Helicobacter in our conventional animal facility. Transgenic animals were weighed two times a week, beginning at 7 weeks of age. Starting at 6 weeks of age mice were evaluated for motor

deficits with a behavioral score system: 0 = Full extension of hind legs away from the lateral midline when the mouse is suspended by tail; the mouse must hold this position for 2 s, and is suspended 2–3 times; 1 = Collapse or partial collapse of leg extension towards lateral midline (weakness) or trembling of hind legs during tail suspension; 2 = Curling of the toes and dragging of at least one limb during walking; 3 = Rigid paralysis or minimal joint movement; foot not used for forward motion; 4 = Mouse cannot stand up in 20 s from either side, euthanasia.

Mice were always treated in blinded fashion.

2.2 TRAM-34 treatment and survival analysis

Male transgenic animals were weighed twice a week from 6 until 18 weeks of age. Then, the animal status and weight was monitored daily. Starting at 7 weeks of age, hSOD1^{G93A} mice were randomly grouped (at least 5 mice per experimental group) for vehicle and TRAM-34 (1-[(2-chlorophenyl)diphenylmethyl]-1*H*-pyrazole treatment. Mice were treated daily (early in the morning) with 120 mg/kg of TRAM-34 or the same amount of vehicle (50 μl, peanut oil, Sigma-Aldrich, St. Louis, MO USA, #P2144) by intraperitoneal injections. The treatment regimen was chosen to reach a CNS concentration of TRAM-34 that effectively inhibits KCa3.1 channels, as previously described (D'Alessandro et al., 2013). TRAM-34 was synthesized as described (Wulff et al., 2000). Animals were treated until the age described in the text or until sacrifice for the survival analysis experiments. Animals were sacrificed when unable to stand up within 20 s after being placed on either side.

2.3 Isolation of lumbar microglia cells

Adult microglia were isolated from the lumbar spinal cord tract of age-matched non-transgenic C57BL/6J wt mice (non-tg *wt*) and hSOD1^{G93A} mice as described in (Yip et al., 2009) with minor modifications. Mice were deeply anesthetized with chloral hydrate (i.p., 400mg/Kg, Carlo Erba Italy, #334085) before being transcardially perfused with phosphate buffered-saline (PBS tablet, Sigma-Aldrich, #P4417). Spinal cords were then flushed out from the spinal canal using a 20 ml syringe filled with PBS and digested with 30 units of papain (15–23 U/mg protein, Sigma-Aldrich, #P3125) for 30 min at 37°C. Tissue was then triturated with a pipette to obtain single cell suspensions, which were applied to 70-μm/40-μm cell strainers and used for the experiments. Purity of isolated microglia was assessed by morphology and surface staining for CD11b^{+}, CD45^{low+}, Ly6G^{-}, Ly6C^{-}. mAbs directly conjugated to PE, PE-Cy7, APC, APC-H7, and PerCP-Cy5.5 fluorochromes and specific for the following antigens (clone name in parentheses) were used: CD45 (104), CD11b (M1/70), Ly6C (HK1.4), and Ly6G (1A8). Antibodies were from eBioscience (Thermo Fisher, Germany) and BioLegend (San Diego, CA). Immunostaining was performed with saturating amounts of Abs for 30 min at 4°C. Purity of isolated microglia cells ranged between 70–90 %, as verified by flow cytometry.

2.4 ROS production

Microglia from the lumbar spinal cord of non-tg *wt* mice were treated for 18h with 5 μM of sodium azide (Acros, part of Thermo Fisher, Germany #190381000) in presence or absence of 2.5 μM of TRAM-34. To evaluate ROS production, cells were extensively washed and

incubated with 10 μM of 2′,7′-Dichlorodihydrofluorescein diacetate (DCF, Sigma-Aldrich, #D6883) for 30 min at 37°C. Cell fluorescence was detected in FL1 channel and analyzed with a FACSCanto II (BD Biosciences). Data were analyzed using FlowJo v9.3.2 software (TreeStar, Ashland, OR, USA).

2.5 Isolation of embryonic mouse MN

MN cultures were obtained from E13 C57BL6/J mice. Pregnant females were euthanized by cervical dislocation and the spinal cords were removed from embryos; tissues were digested with 0.25% Trypsin in Neurobasal medium at 37°C. After 20 min the reaction was stopped by adding trypsin inhibitor and pipetting 10–15 times with a glass Pasteur pipette, until no more cell aggregates were visible. Cells were kept 15 min at RT on a vibration-free surface and centrifuged at 1200 rpm for 10 min; the pellet was resuspended in complete Neurobasal medium (Gibco, part of Thermo Fisher, Germany #10888-022) (2 mM glutamine, 1% B27, 100 U/ml penicillin and 0.1 mg/mL streptomycin) and plated (2×10^5 cells/well) onto poly-L-lysine coated glass cover slips. After nine days in culture, embryonic mouse MNs (2×10^5 cells/well) were co-cultured with adult microglia (non-tg *wt* pre-treated with 5 μM sodium azide (NaN_3) or $hSOD1^{G93A}$ microglia) plated (10^5 cells/well) on poly-L-lysine-coated transwells (Corning, Sigma-Aldrich, USA, 0.4 μm pore size).

2.6 Microglia/MN co-cultures

Co-cultures were treated with the following: 2.5 μM TRAM-34, or DMSO (0.01%, Sigma-Aldrich, USA) as vehicle. After 72 h of co-culture, MN death was measured by immunofluorescence staining using activated caspase 3 antibody (Cell Signaling, Danvers, USA #9661, 1:400), as apoptotic marker, and non-phosphorylated neurofilament H antibody (SMI32 clone, Biolegend, #801701, 1:500), as MN marker. Only double positive cells were counted as dead cells; this number was normalized to the mean of SMI32-positive cells counted in each well.

2.7 Real-time PCR

Total RNA was extracted from lumbar microglia, muscle fibres of non-tg *wt*, vehicle and TRAM-34-treated $hSOD1^{G93A}$ mice following a standard Trizol (Invitrogen, CA, #T9424) protocol, quantified with NanodropOne (Thermo Scientific) and retro-transcripted using IScript Reverse Transcription Supermix (Bio-Rad, #1708841). RT-PCR of genes described was carried out in a I-Cycler IQ Multicolor RT-PCR Detection System (Bio-Rad, #172-5201) using SsoFast Eva Green Supermix (Bio-Rad). Relative gene expression was calculated by ΔΔCT analysis relative to GAPDH expression levels. GAPDH: forward (F), 5′-TCGTCCCGTAGACAAAATGG-3′, reverse (R), 5′-TTGAGGTCAATGAAGGGGTC-3′; IL-1β: F, 5′-GCAACTGTTCCTGAACTCAACT-3′, R, 5′-ATCTTTTGGGGTCCGTCAACT-3′; BDNF: F, 5′-CGGC GCCCATGAAAGAAGTA-3′, R, 5′-AGACCTCTCGAA CCTGCCCT-3′; ARG1:(F), 5′-CTCCAAGCCAAAGTCCTTAGAG-3′, (R) 5′-AGGAGCTGTCATTAGGGACATC-3′; CD163:(F), 5′-TCTGGCTTGACAGCGTTTC-3′, (R) 5′-TGTGTTTGTTGCCTGGATT-3′;FIZZ:(F),5′-CCAATCCAGCTAACTATCCCTCC-3′, (R) 5′-ACCCAGTAGCAGTCATCCCA-3′;IL-6:(F),5′-GATGGATGCTACCAAACTGGA-3′, (R) 5′-TCTGAAGGACTCTGGCTTTG-3′;INOS:(F), 5′-

ACATCGACCCGTCCACAGTAT-3′, (R) 5′-CAGAGGGGTAGGCTTGTCTC-3′;TNF-a: (F), 5′-GTGGAACTGGCAGAAGAG-3′, (R) 5′-CCATAGAACTGATGAGAGG-3′;YM1: (F), 5′-CAGGTCTGGCAATTCTTCTGAA-3′, (R) 5′-GTCTTGCTCATGTGTGTAAGTGA-3′; myogenin (F) 5’-GCACTGGAGTTCGGTCCCA-3’, (R) 5’-GTGATGCTGTCCACGATGGA-3’; atrogyn-1 (F) 5’-GCAGCAGCTGAATAGCATCCA-3’, (R) 5’-GGTGATCGTGAGGCCTTTGAA-3’; AChRγ (F) 5’-GCTCAGCTGCAAGTTGATCTC-3’, (R) 5’-CCTCCTGCTCCATCTCTGTC-3’; AChRε 5’-GCTGTGTGGATGCTGTGAAC-3’, (R) 5’-GCTGCCCAAAAACAGACATT-3’; kccn4 (F) 5’-GGCTGAAACACCGGAAGCTC-3’, (R) 5’-CAGCTCTGTCAGGGCATCCA-3’.

2.8 Behavioral tests

Mice were housed in standard breeding cages at a constant temperature (22 ± 1°C) and relative humidity (50 %), with a 12:12 h light:dark cycle (light on 07.00–19.00 h). Food and water were available ad libitum. Behavioral tests started when mice were 7 weeks old. All animals were handled for at least 5 min/day for 2–3 days before starting the experiments.

2.8.1 Inverted grid test—Mice were placed in the center of a wire grid (40×60cm, suspended 50 cm above a cushioned table) and then the grid was inverted (maximum time allowed 60 s). The time spent hanging on to the grid was measured. (Rinaldi et al., 2013)

2.8.2 Hindlimb Extension Reflex—Mice were suspended by the tail, and scored for hindlimb extension reflex deficits. The scores were recorded from 0 to 2 as follows: 2, normal extension reflex in both hind limbs; 1.5, imbalanced extension in the hind limbs; 1.0, extension reflex in only one hindlimb; 0.5, the absence of any hindlimb extension; and 0, total paralysis. (Ludolph et al., 2010)

2.8.3 Hanging wire test—To perform this test, mice were allowed to grab a horizontal wire with their front paws and the time spent hanging measured (maximum time allowed 60 s). Behavior was scored according to the following scale: 1, hanging onto the bar with both forepaws; 2, in addition to 1, attempted to climb onto the bar; 3, hanging onto the bar with two forepaws and one or both hindpaws; 4, hanging onto the bar with all four paws with tail wrapped around the bar; 5, able to walk on the bar to escape. (Rinaldi et al, 2013)

2.8.4 Rotarod test—Motor coordination, strength and balance were assessed using a rotarod apparatus (Ugo Basile, Gemonio Italy, #47650). Animals were placed onto the cylinder at a constant speed of 15 rpm. The arbitrary cut-off time was 300 s., and the longest latency was recorded.

2.8.5 Grip strength test—The apparatus consisted of a grip strength meter (Ugo Basile, #47200), complete with a force transducer and a grasping device (grid for measurement of the four limbs). The mouse was held at the base of the tail and allowed to grab the grid with either four limbs. The mouse was then pulled gently backwards until it released its grip. The peak force of each trial was taken as a measure of the grip strength.

2.9 Immunofluorescence

Spinal cord slices were prepared from hSOD1^{G93A} and non-tg *wt* mice treated with vehicle or TRAM-34 as described. Spinal cord sections (20 μm) were washed in PBS, blocked (3% goat serum in 0.3% Triton X-100) for 1 h, at RT, and incubated overnight at 4°C with specific antibodies diluted in PBS containing 1% goat serum and 0.1% Triton X-100. The sections were incubated with the following primary Abs: Iba1 (Wako, Osaka Japan, #019-19741, 1:500), GFAP (Novus Biologicals, Littleton USA, #NB300-141, 1:500), SMI-32 (BioLegend, 1:500) and cleaved caspase-3 (Cell Signaling, 1:400). After several washes, sections were stained with the fluorophore-conjugated antibody and Hoechst for nuclei visualization and analyzed using a fluorescence microscope. For Iba1/SMI-32 staining, coronal sections were first boiled for 20 min in citrate buffer (pH 6.0) at 95–100°C. Quantification of Iba1 and GFAP immunoreactivity was performed on lumbar spinal cord sections (12 serial coronal sections for each animal, in each group, covering the entire L3–L5 segments), using MetaMorph 7.6.5.0 image analysis software (Molecular Device, San Jose USA), after background subtraction. Iba or GFAP immunoreactivity was measured as the ratio of the area occupied by fluorescent cells (thresholded area) versus the total ventral horn area. At least 5 animals per condition were analyzed.

Images were digitized using a CoolSNAP camera (Photometrics, Tucson USA) coupled to an ECLIPSE Ti-S microscope (Nikon, Tokio Japan) and processed using MetaMorph 7.6.5.0 image analysis software (Molecular Device, San Jose USA). Signal co-localization was analyzed measuring the average fluorescence intensity (pixel) of merged signals.

2.10 Motor Neuron survival evaluation

For MN survival, the whole ventral horns of lumbar spinal cord were photographed at ×20 magnification and digitized using a CoolSNAP camera (Photometrics) coupled to an ECLIPSE Ti-S microscope (Nikon) and processed using MetaMorph 7.6.5.0 image analysis software (Molecular Device). The number of MNs was evaluated counting only SMI32-positive cells with typical morphology triangular shape, single well-defined axon, large body diameter (≥ 20 μm) and intact axons and dendrites. This was done in 12 serial slices for each animal and data normalized with respect to non-tg wild-type mice, where the number of healthy MNs was taken as 100 %.

2.11 Skeleton analysis

Microglia from sections of lumbar ventral horns were analyzed by confocal microscopy using IBA1 signal and skeletonized to assess cell morphology. Twenty μm z-stacks were acquired at 0.5 μm intervals using an FV10i laser scanning microscope (Olympus, Tokyo Japan) at ×60 objective. Cell morphology was measured using a method adapted from Morrison (2013). Maximum intensity projections for the IBA1 channel of each image were generated, binarized, and skeletonized using the Skeletonize 2D/3D plugin in ImageJ, after which the Analyze Skeleton plugin (http://imagej.net/AnalyzeSkeleton) was applied. The average branch number (process end points per cell) for each image with a voxel size exclusion limit of 150 was applied. The number of single and multiple junction points was additionally calculated to give an indication of branching complexity. The areas of the soma

and the scanning domain, defined as the perimeter within which individual cells project their dynamic processes, were measured for each cell.

2.12 Fibre preparation

Fibres were obtained from the FDB muscles of hSOD1^{G93A} and non-tg *wt* mice hind-limbs. The dissected muscles were incubated with Type I collagenase (2 mg/ml, Sigma) for 45 min at 37°C in MEM (Gibco, #11095-080) digestion medium (Sodium Pyruvate 1mM + FBS 0.2% + Pen Strep 2%, Sigma). After equilibrating in S-MEM (Gibco, #11380-037) Ca2+-free dissociation medium (Sodium Pyruvate 1mM + FBS 0.5% + Pen Strep 2% + HEPES 20mM, Sigma) for 15 min at 37°C, the muscle fibres were mechanically dissociated using fire polished glass pipettes and P100 micropipette. For recordings, a bunch of single fibres was transferred on ECM (3.33 mg/mL, Sigma-Aldrich, USA) coated glass slide and incubated at 37°C for 15 min. The fibres remained viable for at least 4–5 h.

2.13 Neuromuscular junction evaluation

Mice treated as above were deeply anaesthetized before being transcardially perfused with PBS. *Tibialis anterior* muscles were dissected out and snap-frozen in cooled isopentane. Muscles were gently stretched on a Sylgard coated Petri dish and fixed with paraformaldehyde 4% in PBS for 60 min at RT. For AChR staining, the fixed muscles were incubated with rhodamine-conjugated alpha-bungarotoxin (6 mg/ml, Molecular Probes, B13423) in FBS-supplemented DMEM 20% for 50 min at 37°C. Muscle were extensively washed with FBS-supplemented DMEM 20%, then with PBS. Twenty-micrometer serial longitudinal cryosections were collected on poly-lysine coated objective slides (VWR International, Radnor USA) for the quantitative evaluation of NMJ status. Images were digitized using a CoolSNAP camera (Photometrics) coupled to an ECLIPSE Ti-S microscope (Nikon) and processed using MetaMorph 7.6.5.0 image analysis software (Molecular Device). Images of acetylcholine receptors (AChRs) immuno-stained with α-BTX were used for the quantification of NMJ fragmentation. Fragmentation of NMJ was defined as several AChR clusters in small islands with round shape. Average numbers of AChR fragments per NMJ were evaluated. For the quantitative evaluation, about 130 NMJs for each group were analyzed.

2.14 Cell-attached recordings and analysis

Single-channel currents were recorded at room temperature (24–26 °C) in the cell-attached mode from dissociated muscle fibres from hSOD1^{G93A} or non-tg mice and bathed in dissociation medium without divalent ions to prevent contractions. Glass pipettes (3–5 MΩ) pulled with a vertical puller (PC-10, Narishige) were filled with divalent-free NES (NaCl 140mM, KCl 2.8mM, Glucose 10mM, HEPES/NaOH 10mM, pH 7.3, 295–300 mOsm) plus ACh 200nM and were connected to a low-noise amplifier (Multiclamp 700B amplifier, Molecular Devices, USA). Data were sampled at 20 kHz and analysed after Gaussian digital filtering at 6 kHz, using a threshold-crossing method (pClamp v. 10.0 software, Axon Instruments), with the detection threshold for channel events set to half-amplitude. Events briefer than 120 μs were incompletely resolved and therefore excluded from the analysis. The histogram of channel amplitudes was adequately fitted by one or two Gaussian distributions and slope conductances were calculated by least-squares linear fitting of

unitary current (*i*)/voltage (*V*) relationships. Only single openings were used to calculate the mean channel amplitude and the apparent open duration (τop), which was measured at half-amplitude for each event. The kinetic properties of ACh-evoked events were compared at an estimated patch potential of –90±10 mV. Only patch with at least 1000 events were used to perform open channel duration analysis. Results are given as mean ± SEM. The significance of differences was tested by using one-way ANOVA ($P<0.05$) and Fisher's test.

2.15 Statistical analysis

Data are expressed as the mean ± S.E.M. Student's t-test, paired t-test, Fisher's test, one-way or two-way analysis of variance (ANOVA) was performed. A value of $P< 0.05$ was considered significant. All statistical analyses were carried out using the Sigma Plot 11.0 Software (Systat Software GmbH, Erkrath, Germany). Mouse survival was analyzed with the Kaplan–Meier graph followed by log-rank statistics. The sample size (n) was chosen differently for experiments of animal survival, behavioural tests, electrophysiology, etc, considering the following relation: $n \geq 2\sigma^2(z_\alpha/D)^2$ where sigma is substituted by an estimate of variance (s2); alpha is at 0.05 (and $Z\alpha=-2$) and D is the difference among treatments.

3. Results

3.1 KCa3.1 channels modulate spinal microglia in hSOD1^{G93A} mice

In the CNS, KCa3.1 is highly expressed in activated microglia (Kaushal et al., 2007). To investigate the possible involvement of KCa3.1 channels in modulating the phenotype of microglia in the fully symptomatic phase of ALS, we first analyzed the mRNA level of *kcnn4*, by quantitative real time PCR (qRT-PCR), in microglia isolated from the lumbar region of the spinal cord of 18 week-old hSOD1^{G93A} mice. Preliminarily, we confirmed that these cells have increased expression of selected inflammatory genes and reduced expression of anti-inflammatory ones (Fig.1A, left), as previously described in ALS mice (Liao et al., 2012; Apolloni et al., 2016). We found that hSOD1^{G93A} microglia express high level of *kcnn4* (7.54 fold increase in comparison with age-matched non-tg *wt* mice), suggesting that KCa3.1 channels could play a role in the pro-inflammatory microenvironment observed in ALS (Fig.1A, right). To directly evaluate the role of KCa3.1 channel activity in modulating microglia phenotype, hSOD1^{G93A} mice were treated with TRAM-34 (daily, 120mg/kg) from 7 weeks of age (pre-symptomatic stage) until 18 weeks (fully symptomatic stage) (Fig.1B, **top**). The long term treatment is not toxic and does not induce changes in body weight, haematology, blood chemistry or necropsy of any major organs, either in mice or rats (Toyama et al., 2008; Chen et al., 2011). After this period, microglial cells were isolated and analyzed as in A. As shown in figure 1B, pharmacological KCa3.1 inhibition changed the expression level of several inflammatory genes in hSOD1^{G93A} microglia (**left**), decreasing *inos, tnf-α, il-1β, il-6* and *p2yr6* expression compared to microglia obtained from vehicle-treated hSOD1^{G93A} mice (dotted line). Interestingly, treatment with TRAM-34 also reduced *kcnn4* expression (to 0.27 ± 0.09 fold) compared to vehicle-treated mice. In contrast, KCa3.1 inhibition increased the expression of the anti-inflammatory genes *arg1, cd163, sosc3, ym1, bdnf* and *p2yr12* (Fig.1B, **right**). As a control, we also analyzed gene expression in microglia isolated from the lumbar spinal cord of non-tg *wt* mice, upon vehicle

and TRAM-34 (four weeks) treatment. Results obtained indicate that KCa3.1 inhibition induces significant increases of *arg1* and *ym1* genes (see Supplementary table 2).

Immunofluorescence analysis of the spinal cord, revealed that KCa3.1 inhibition, in hSOD1^{G93A} mice (scheme of mice treatment in Fig.1C, **top**), significantly decreased Iba1 and GFAP staining in the L3–L5 regions, compared to vehicle-treated mice (Fig.1C, **center and bottom**), further confirming the induction of a reduced inflammatory environment. Iba1-positive cells in these spinal sections were also analyzed for morphological changes by performing skeleton analysis to quantify single cell shape. The data summarized in figure 1D, reveal that Iba-1 positive cells from TRAM-34 treated mice had significantly smaller somas, bigger scanning domains and higher average branch numbers. Skeleton analysis also evidenced higher number of junctions and more triple as well as quadruple junction points, when compared to vehicle-treated animals. Taken together, these results indicate that KCa3.1 inhibition shifts spinal microglia of hSOD1^{G93A} mice towards an anti-inflammatory phenotype and increases the active surveillance that microglia exert in their competence domains. These data consistently support our hypothesis of KCa3.1 involvement in microglia modulation in ALS and further prompted us to verify if channel inhibition could significantly impact disease progression.

3.2 Inhibition of KCa3.1 has beneficial effects in hSOD1^{G93A} mice

To assess the possible beneficial effects of KCa3.1 inhibition on ALS progression, we treated hSOD1^{G93A} mice daily with TRAM-34 or vehicle (as detailed above) from 7-weeks of age until sacrifice (Fig.2A). Mice were evaluated during the treatment period for changes in weight, locomotor activity, muscle strength, motor coordination and survival. As shown in Fig.2B, TRAM-34 treatment significantly increased body weight from week 13 to the end stage. Disease onset was retrospectively determined as the age when these mice reached their maximal body weight: KCa3.1 inhibition delayed disease onset of about 3 weeks in hSOD1^{G93A} mice (Fig.2C). In addition, KCa3.1 inhibition increased survival time (Fig.2D) compared to vehicle treated mice and significantly prolonged the mean survival time post-paralysis, assessed as the age when mice failed to complete the Rotarod test (Fig.2E).

We also tested locomotor ability, muscle strength and motor coordination in vehicle and TRAM-34 treated hSOD1^{G93A} mice. The results of these experiments show that in the hanging wire test, the TRAM-34 treated mice (Figures 2F and 2G), for the time investigated, always performed with higher scores and spent more time hanging compared to controls. Of note, the TRAM-34-treated mice never reached the lowest score (1) during the symptomatic stage (13–18 weeks), showing a very good, preserved, locomotor ability. In the inverted grid test (Fig.2H), the average latency to fall recorded for TRAM-34-treated mice was longer compared to vehicle-treated mice at all the time point analyzed. hSOD1^{G93A} mice were further tested for motor coordination and balance using a Rotarod apparatus. Mice treated with TRAM-34 performed better on the Rotarod (Fig.2I) and continued to do so until week-21. The grip strength data (Fig.2L) obtained for TRAM-34 treated mice showed that the rate of muscle deterioration was lower compared to vehicle treated mice, suggesting a slower disease progression. In addition, mice treated with TRAM-34 showed a preserved hind-limb extension reflex (Fig.2M) compared to vehicle treated mice from the beginning of

the symptomatic stage. Taken together, these results show that KCa3.1 inhibition significantly delays symptom onset, suggesting that these channels are involved in accelerating disease progression.

3.3 Motor neurons are protected by selective KCa3.1 inhibition in hSOD1^{G93A} mice

In order to investigate if the activity of KCa3.1 channels in microglia could be involved in MN death in ALS, another group of hSOD1^{G93A} mice were treated with TRAM-34 or vehicle from the pre-symptomatic until the disease onset phase (from 7 weeks to 16 weeks of age, scheme on top of Fig.3A) when the spinal cords were collected. MNs in the ventral horns of the spinal cord regions L3–L5 were stained with an antibody against the non-phosphorylated neurofilament H (SMI32) (a MN marker) and cells with large cell body (diameter ≥ 20 μm) were counted. The mean number of MNs in *wt* animals was taken as control value. As shown in figure 3A, KCa3.1 inhibition, in hSOD1^{G93A} mice, increased MN survival (TRAM-34 52.00 ± 3.13 %, vehicle 38.26 ± 1.38% *vs wt* 100 ± 1.09%). Taking advantage of a microglia/MN co-culture system, we then evaluated the specific communication between MN and microglial cells. To this aim, primary adult microglia isolated from symptomatic (16 weeks) or end-stage (>20 weeks) hSOD1^{G93A} mice were co-cultured with MNs isolated from the spinal cord of mouse embryos (E13) and treated with 2.5 μM TRAM-34 or vehicle (DMSO). After 72 h of co-culture, MN death was measured by staining with SMI32 and the activated caspase 3 antibody, as an apoptosis marker. As shown in figure 3B, co-cultures with both symptomatic and end-stage hSOD1^{G93A} microglia induced MN death (apoptotic MNs in symptomatic and end-stage were respectively, 83.3 ± 2.5 % and 78.1 ± 1.6 %), while co-culture with *wt* microglia did not (apoptotic MNs were 17.8± 1.7%), in accordance with (Frakes et al 2014). In the presence of the KCa3.1 inhibitor, MN death induced by hSOD1^{G93A} microglia was prevented or significantly decreased (symptomatic microglia: 12.1 ± 1.4 %; end-stage: 28± 1.5 %; *wt*: 17.8± 1.7 %). These data indicate that KCa3.1 channel activity on microglia influences microglia-MN communication, increasing MN death in hSOD1^{G93A} mice.

3.4 Selective KCa3.1 inhibition counteracts ROS-induced microglia neurotoxicity

Mitochondrial reactive oxygen species (ROS) play a prominent role in the oxidative stress observed in ALS (Barber et al., 2010). To investigate whether KCa3.1 activity modulates ROS production in microglia, we used sodium azide (NaN_3), an inhibitor of the electron transport chain, to increase ROS levels (Ye et al., 2016). Microglia (from *wt* mice) were therefore treated with 5μM NaN_3 for 18 h, in the presence or absence of TRAM-34 (2.5μM) or vehicle, and mitochondrial ROS production was evaluated by loading cells with 10μM 2′, 7′-dichlorofluorescin diacetate (DCF). Alternatively, microglia were co-incubated for additional 24 h with primary MN to evaluate neurotoxicity.

The data reported in figure 4A show that NaN_3 treatment induced ROS production in microglia and that KCa3.1 channel inhibition reduced it, as measured by cytofluorimetric analysis (DCF^+ microglial cells were: NaN_3: 5.4±0.3%; NaN_3+TRAM-34: 2.8±0.4%). In accordance, MN death (measured as above) increased when MNs were co-cultured for 48h with microglia pre-treated with NaN_3 (Fig.4B, 19.06 ± 0.8% control microglia; 71.6 ± 2.04% NaN_3 microglia). Neurotoxicity was abolished when MNs were co-cultured with

microglia pre-treated with NaN_3/TRAM-34 (22.06 ± 1.98%), suggesting that KCa3.1 function is involved in sustaining ROS production in microglia. As shown in the first two bars of Figure 4B, TRAM-34 exerted a minor neuroprotective action also in control co-cultures.

3.5 Selective KCa3.1 inhibition preserves neuromuscular junction (NMJ) functionality

In hSOD1^{G93A} mice, muscle force and motor coordination start to decline at about 10–11 weeks, with clear evidence of NMJ alterations (Dobrowolny et al., 2011). The functional data reported above suggest that NMJ is preserved for longer time in animals treated with TRAM-34. Therefore, we performed morphological and functional analysis of NMJ in hSOD1^{G93A} mice treated with TRAM-34 or vehicle from 7-to 16-weeks of age (Fig.5A, **left**). To evaluate the NMJ morphology/integrity, the *tibialis anterior* (TA) muscle was isolated, stretched and fixed. Bundles of muscle fibres were stained with alpha-bungarotoxin (α-BTX) and analyzed for NMJ fragmentation. In symptomatic, vehicle treated mice, the average acetylcholine receptor (AChR) -rich fragments per NMJ were 2.07 ± 0.18 (vehicle n=3, 136 NMJs) and in TRAM-34-treated hSOD1^{G93A} mice this value drops to 0.96 ± 0.06 (TRAM-34 n=4, 135 NMJs), not dissimilar to what was observed in non-tg age matched mice (0.4 ± 0.06 per NMJ, non-tg n=3, 148 NMJs) (see Fig.5A, center and right for representative images).

Several signaling pathways contribute to skeletal muscle atrophy in ALS patients as well as in hSOD1^{G93A} mice (Krasnianki et al., 2005; Dupuis et al., 2006). Increased expression of the late myogenic transcription factor myogenin *(myf4)* and the muscle-specific E3 ubiquitin ligase (*atrogin 1*) were detected in both mouse (Manzano et al., 2011) and human ALS muscles (Léger et al., 2006). As shown in figure 5B, the mRNA level of *atrogin1* and *myogenin* were reduced in TRAM-34-*vs* vehicle-treated hSOD1^{G93A} mice (respectively 0.27-fold and 0.69-fold; vehicle n=3 TRAM-34 n=4 *atro gin* *p<0.002 *vs* vehicle, *myogenin* ***p<0.001 *vs* vehicle).

We also measured the expression level of AchRγ and ε subunits in vehicle and TRAM-34 treated mice, an index for NMJ denervation (Martinou et al., 1991). In hSOD1^{G93A} muscle, at the paralysis stage, expression of AChRγ was upregulated, in agreement with previous studies (Krasnianski et al., 2005). Data reported in figure 5C show a decreased (0.59-fold) AChRγ and an increased (3.08-fold) AChRε expression in TRAM-34 treated hSOD1^{G93A} mice (vehicle n=4 TRAM-34 n=6, AChRγ ***p<0.001 *vs* vehicle, AChRε ***p<0.001 *vs* vehicle).

To assess whether TRAM-34 treatment preserves AChR functionality, patch-clamp recordings were performed in acutely dissociated flexor *digitorum brevis* (FDB) muscle fibres. The single channel properties of AChRs were investigated under cell-attached conditions at the end-plate region. To improve the mechanical stability of the patches, recordings were performed with pipette solutions free of Ca^{2+} and Mg^{2+} ions. In all recordings obtained from *wt* mice (13 fibres/5 animals) only one population of ACh-activated channels was observed (Fig.5D, **left**). Unitary channel slope conductance was 78.23 ± 1.71 pS, as expected for AChRε in the absence of divalent cations. By contrast, in 7 out of 11 recordings obtained in end-plates from 16-weeks old, vehicle treated SOD1^{G93A}

mice (5 mice) two population of channels, differing in amplitude, were observed (Fig.5D, **middle**). Slope conductances were 53.15 ± 1.96 pS (23%) and 82.56 ± 1.28 pS (77%), typical values for γ- and ε- containing AChRs, respectively. As expected, based on the data reported above, only one population of ACh-evoked channel openings was detected in 10 out of 12 recordings (6 mice) in TRAM-34 treated hSOD1^{G93A} mice (Fig. 5D, **right**). Channel slope conductance was 79.22 ± 1.75 pS. In 2 fibres, a small fraction of openings belonged to a population with 38.1 and 59.34 pS slope conductance. Thus, the number of fibres expressing AChRγ channel was significantly reduced in TRAM-34-treated hSOD1^{G93A} mice (p=0.0009, Fisher's exact test). The slope conductance of AChRε showed no statistically significant difference among groups. The histograms of AChRε channel open duration were fitted to the sum of three exponential components which did not differ among the groups (suppl. Table 1) showing that the function of AChR channels is not perturbed in hSOD1^{G93A} mice.

4. Discussion

Increasing evidence supports the hypothesis that in ALS, a neuroinflammatory microenvironment support MN degeneration (Fiala et al., 2010; Puentes et al., 2016; Pasetto et al., 2017; Vallarola et al., 2018). In this paper we demonstrated that in hSOD1^{G93A}, a mouse model of fALS, spinal microglia overexpress the calcium-activated potassium channel, KCa3.1, and that blockade of this channel induces a significant delay in the appearance of all symptoms, preserving motor function and slowing disease progression. In the CNS, KCa3.1 is expressed by microglia and transformed cells (Kaushal et al., 2007; Manzano et al., 2011) and, in a model of spinal cord injury, it has been detected on neurons and astrocytes (Bouhy et al., 2011). In our experimental conditions, we never measured KCa3.1 activity or expression in spinal MN of *wt* and hSOD1^{G93A} mice. KCa3.1 channels expressed on microglial cell play important roles in neurodegenerative diseases and in brain tumors modulating cell phenotype (D'Alessandro et al., 2018; Nguyen et al., 2017). The expression of the mutant SOD1^{G93A} gene in microglia has been related to MN degeneration and to ALS progression (Boilléè et al., 2006; Beers et al., 2006). Here we tested the hypothesis that the activity of KCa3.1 channels is associated to a pro-inflammatory phenotype of microglial cells, that favors MN death and disease progression. This is the first study that investigate the role of KCa3.1 channels in ALS, and we demonstrated that the chronic treatment of hSOD1^{G93A} mice with the KCa3.1 channel inhibitor TRAM-34 modulates the phenotype of spinal microglia. In both ALS patients and mouse models, the expression of pro-inflammatory genes increases (Lu et al., 2016; Lee et al., 2016), while anti-inflammatory genes decrease (Liao et al., 2012; Apolloni et al., 2016; Lewis et al., 2014). In line with our hypothesis, we observed that TRAM-34 treatment reverts this trend, increasing the anti-inflammatory (such as *arg1, cd163, socs3*, and *ym1*) and decreasing several pro-inflammatory genes (*il1β, tnf-α, il6* and *inos*) in spinal microglia of hSOD1^{G93A} mice. Interestingly, KCa3.1 blockade induces some phenotypic changes also in microglia of *wt* mice, increasing the expression of *arg1* and *ym1* genes, further confirming the role of this channel in the modulation of microglia phenotype. Like in other neurodegenerative diseases and similarly to brain tumors, microglia play a dual role in early and late stages of ALS (Ferreira et al., 2015). A recent data-driven experimental approach revealed a link between

microglia and the development of MN pathology, identifying soluble TREM2 in the CSF as a putative marker of disease progression (Cooper-Knock et al., 2017).

Expression of other genes, potentially relevant to microglia function and MN death, is also altered by blockade of KCa3.1 channels, in agreement with the induction of an anti-inflammatory phenotype. For example, the expression of the *p2yr6* gene is increased in spinal hSOD1^{G93A} microglia (D'Ambrosi et al., 2009), and we observed that TRAM-34 treatment prevents this overexpression. P2Y6 purinergic receptors are involved in microglia phagocytosis (Koizumi et al., 2007; Brown et al., 2014) and related to MN loss in ALS (D'Ambrosi et al., 2009). The phagocytic activity of microglia has debated roles in ALS, where it controls the removal of MNs at different stages of the disease (D'Ambrosi et al., 2009; Butovsky et al., 2014). Interestingly, recent data (Paolicelli et al., 2017), demonstrate that TDP-43, a gene associated with ALS, controls microglia phagocytic activity.

The expression of BDNF, insulin-like growth factor-1 (IGF-1), fibroblast growth factor-2 (FGF-2), and vascular endothelial growth factor are all downregulated in ALS patients (Shruthi et al., 2017; Ohsawa et al., 2010). We observed that the expression of the neuroprotective factor *bdnf* is boosted in hSOD1^{G93A} microglia by inhibiting KCa3.1 activity. In line with the gene expression data, spinal microglia of TRAM-34 treated hSOD1^{G93A} mice at symptomatic stage are less amoeboid, have smaller soma and higher branching complexity. These morphology data reveal that blockade of KCa3.1 activity restores the patrolling activity of microglia in hSOD1^{G93A} mice. This is in accordance with the higher expression of the metabotropic receptor P2Y12, known to be involved in microglia process mobility (Appel et al., 2011).

Microglia-MN communication in hSOD1^{G93A} mice also benefits from the blockade of KCa3.1 channels. The observed neuroprotective effect is likely due to the combination of a reduced inflammatory phenotype and an increased production of the neurotrophin BDNF. Taken together, these data confirm a key role for KCa3.1 in mediating a pro-inflammatory microglia behavior, as described in other CNS diseases, such as AD, multiple sclerosis, spinal cord injury and ischemia (Maezawa et al., 2011; Moloney et al, 2014; Kaushal et al., 2007; Chen et al., 2016).

These findings are associated with a reduced NMJ damage, seen as less fragmented and better-preserved structure, together with a decreased muscle denervation, demonstrated by a shift in the expression of the γ and ε AChR subunits in hSOD1^{G93A} mice treated with TRAM-34. We interpret the enhanced expression of the ε AChR subunit as a consequence of ongoing denervation/reinnervation cycles in TRAM-34 treated mice. Functional recordings on FDB fibres confirmed the expression data. In addition, KCa3.1 inhibition induced a decrease in the expression markers of atrophy normally detected in ALS muscle (Dobrowolny et al., 2011), such as myogenin and the E3 ubiquitin ligase atrogin 1.

Degeneration of NMJs together with multiple pathogenic mechanisms such as oxidative stress, aberrant protein aggregation, defective axonal transport, neuroinflammation and mitochondrial dysfunction, all contribute to MN failure in ALS (Philips et al., 2011; Barber et al., 2010; Blokhuis et al., 2013; Barber et al., 2006). In particular, mitochondrial ROS play

a prominent role in the oxidative stress observed in ALS (Barber et al., 2010). We used low concentrations of sodium azide to block the electron transport chain and to induce effects on microglia neurotoxic properties (see Ye et al., 2016), and observed that KCa3.1 inhibition prevented the consequent increase in ROS production in microglial cells. Notably, in addition to the plasma membrane, KCa3.1 (and other Ca^{2+} activated potassium channels such as KCa1.1) are also expressed in the inner membrane of the mitochondria in transformed cells and cardiomyocytes (De Marchi et al., 2009; Aldakkak et al., 2010). KCa1.1 activation increases respiration and ROS generation in cardiac cells providing protection against ischemia and reperfusion (IR) injury (Stowe et al., 2006). We hypothesize that, at least the effect of KCa3.1 inhibition on ROS production, could be partially due to the perturbation of K^+ homeostasis between the mitochondrial matrix and the inter membrane space.

It has been shown that, in GBM, histamine activates KCa3.1 channels through cell hyperpolarization, which in turn induces Ca^{2+} influx (Fioretti et al., 2009); clemastine, a histamine receptor (H1R) antagonist, ameliorates ALS pathology modulating inflammatory parameters (Apolloni et al., 2016). Our results are in accordance with a possible mechanism where histamine, released by peripheral mast cells, activates KCa3.1; blocking H1R would also reduce KCa3.1 activity, thus affecting ALS progression.

4.1 Conclusions

In conclusion, our data indicate that the blockade of KCa3.1, when initiated in the pre-symptomatic stage of the disease, elicits broad protective effects in $hSOD1^{G93A}$ mice inducing: i) anti-inflammatory phenotype in microglia, that re-acquire a proper scanning domain; ii) reduced MN degeneration; iii) an overall delay of disease onset and motor dysfunction and iv) increased mean survival time. Overall, these data describe, for the first time, a critical role for KCa3.1 activity in modulating ALS onset and progression, at least in the $hSOD1^{G93A}$ murine model investigated here. It remains to be clarified: i) whether the effect of the blockade of KCa3.1 on $hSOD1^{G93A}$ mice could be relevant in other familiar forms of ALS, and in sALS; ii) the involvement of other target cells such as immune cells or other parenchymal cells. As a potential future application, it is worth to mention that a molecule structurally related to TRAM-34, Senicapoc®, which advanced into Phase-3 clinical trials, has been proven safe in humans (Ataga et al., 2011). Our data demonstrate that KCa3.1 is a potential target to counteract neuroinflammation and neuromuscular degeneration, at least in familial ALS.

Supplementary Material

Refer to Web version on PubMed Central for supplementary material.

Acknowledgments

The authors thank Maria Teresa Ciotti for embryonal motor neuron cultures. This work was supported by Italian Ministry of University and Research [PRIN 2015] to C.L.; by the National Institute of Health [R01 NS098328 (NINDS)] to H.W. C.L is fellow of the Synanet Network (Twinning Project H2020).

References

Aldakkak M, Stowe DF, Cheng Q, Kwok WM, Camara AK. Mitochondrial matrix K+ flux independent of large-conductance Ca2+-activated K+ channel opening. Am J Physiol Cell Physiol. 2010; 298:C530–C541. [PubMed: 20053924]

Almer G, Vukosavic S, Romero N, Przedborski S. Inducible nitric oxide synthase up-regulation in a transgenic mouse model of familial amyotrophic lateral sclerosis. J Neurochem. 1999; 72(6):2415–25. [PubMed: 10349851]

Apolloni S, Fabrizio P, Parisi C, Amadio S, Volonte C. Clemastine confers neuroprotection and induces an anti-inflammatory phenotype in SOD1(G93A) mouse model of amyotrophic lateral sclerosis. Mol Neurobiol. 2016; 53:518–531. [PubMed: 25482048]

Appel SH, Zhao W, Beers DR, Henkel JS. The microglial-motoneuron dialogue in ALS. Acta Myol. 2011; 30(1):4–8. [PubMed: 21842586]

Ataga KI, Reid M, Ballas SK, Yasin Z, Bigelow C, James LS, Smith WR, Galacteros F, Kutlar A, Hull JH, Stocker JW. Study Investigators. Improvements in haemolysis and indicators of erythrocyte survival do not correlate with acute vaso-occlusive crises in patients with sickle cell disease: a phase III randomized, placebo-controlled, double-blind study of the Gardos channel blocker senicapoc (ICA-17043). Br J Haematol. 2011; 153:92–104. [PubMed: 21323872]

Barber SC, Mead RJ, Shaw PJ. Oxidative stress in ALS: a mechanism of neurodegeneration and a therapeutic target. Biochim Biophys Acta. 2006; 1762(11–12):1051–67. [PubMed: 16713195]

Barber SC, Shaw PJ. Oxidative stress in ALS: key role in motor neuron injury and therapeutic target. Free Radic Biol Med. 2010; 48(5):629–41. 2010. [PubMed: 19969067]

Beers DR, Henkel JS, Xiao Q, Zhao W, Wang J, Yen AA, Siklos L, McKercher SR, Appel SH. Wild-type microglia extend survival in PU. 1 knockout mice with familial amyotrophic lateral sclerosis. Proc Natl Acad Sci U S A. 2006; 103:16021–16026. [PubMed: 17043238]

Blokhuis AM, Groen EJ, Koppers M, van den berg LH, Pasterkamp RJ. Protein aggregation in amyotrophic lateral sclerosis. Acta Neuropathol. 2013; 125:777–794. [PubMed: 23673820]

Bogaert E, d'Ydewalle C, Van Den Bosch L. Amyotrophic lateral sclerosis and excitotoxicity: from pathological mechanism to therapeutic target. CNS Neurol Disord Drug Targets. 2010; 9(3):297–304. [PubMed: 20406181]

Boillée S, Yamanaka K, Lobsiger CS, Copeland NG, Jenkins NA, Kassiotis G, Cleveland DW. Onset and progression in inherited ALS determined by motor neurons and microglia. Science. 2006; 312:1389–1392. [PubMed: 16741123]

Bouhy D, Ghasemlou N, Lively S, Redensek A, Rathore KI, Schlichter LC, Samuel D. Inhibition of the Ca2+-dependent K+ channel, KCNN4/KCa3.1, improves tissue protection and locomotor recovery after spinal cord injury. J. Neurosci. 2011; 31:16298–16308. [PubMed: 22072681]

Brown GC, Neher JJ. Microgli al phagocytosis of live neurons. Nature Reviews. Neuroscience. 2014; 15:209–216. [PubMed: 24646669]

Butovsky O, Jedrychowski MP, Cialic R, Krasemann S, Murugaiyan G, Fanek Z, Greco DJ, Wu PM, Doykan CE, Kiner O, Lawson RJ, Frosch MP, Pochet N, Fatimy RE, Krichevsky AM, Gygi SP, Lassmann H, Berry J, Cudkowicz ME, Weiner HL. Targeting miR-155 restores abnormal microglia and attenuates disease in SOD1 mice. Ann Neurol. 2014; 77:75–99. DOI: 10.1002/ana.24304 [PubMed: 25381879]

Chen YJ, Nguyen HM, Maezawa I, Grössinger EM, Garing AL, Köhler R, Jin LW, Wulff H. The potassium channel KCa3.1 constitutes a pharmacological target for neuroinflammation associated with ischemia/reperfusion stroke. J Cereb Blood Flow Metab. 2016; 36(12):2146–2161. [PubMed: 26661208]

Chen YJ, Raman G, Bodendiek S, O'Donnell ME, Wulff H. The KCa3.1 blocker TRAM-34 reduces infarction and neurological deficit in a rat model of ischemia/reperfusion stroke. J Cereb Blood Flow Metab. 2011; 31:2363–2374. [PubMed: 21750563]

Choi CI, Lee YD, Gwag BJ, Cho SL, Kim SS, Suh-Kim H. Effects of estrogen on lifespan and motor functions in female hSOD1 G93A transgenic mice. J Neurol Sci. 2008; 268(1–2):40–47. [PubMed: 18054961]

Cooper-Knock J, Gren C, Altschuler G, Wei W, Bury JJ, Heath PR, Wyles M, Gelsthorpe C, Highley JR, Lorente-Pons A, Beck T, Doyle K, Otero K, Traynor B, Kirby J, Shaw PJ, Hide WA. A data-driven approach links microglia to pathology and prognosis in amyotrophic lateral sclerosis. Acta Neuropathol Commun. 2017; 5(1):23. [PubMed: 28302159]

Cozzolino M, Carrì MT. Mitochondrial dysfunction in ALS. ProgNeurobiol. 2012; 97(2):54–66.

D'Ambrosi N, Finocchi P, Apolloni S, Cozzolino M, Ferri A, Padovano V, Pietrini G, Carrì MT, Volonté C. The proinflammatory action of microglial P2 receptors is enhanced in SOD1 models for amyotrophic lateral sclerosis. J Immunol. 2009; 183:4648–4656. [PubMed: 19734218]

D'Alessandro G, Catalano M, Sciaccaluga M, Chece G, Cipriani R, Rosito M, Grimaldi A, Lauro C, Cantore G, Santoro A, Fioretti B, Franciolini F, Wulff H, Limatola C. KCa3.1 channels are involved in the infiltrative behavior of glioblastoma in vivo. Cell. Death Dis. 2013; 4:e773. [PubMed: 23949222]

D'Alessandro G, Limatola C, Catalano M. Functional roles of the Ca2+-activated K+ channel, KCa3.1, in brain tumors. Curr Neuropharmacol. 2018 [2017 Jul 13]

De Marchi U, Sassi N, Fioretti B, Catacuzzeno L, Cereghetti GM, Szabò I, Zoratti M. Intermediate conductance Ca2+-activated potassium channel (KCa3.1) in the inner mitochondrial membrane of human colon cancer cells. Cell Calcium. 2009; 45(5):509–16. [PubMed: 19406468]

Dobrowolny G, Aucello M, Musarò A. Muscle atrophy induced by SOD1G93A expression does not involve the activation of caspase in the absence of denervation. Skelet Muscle. 2011; 1(1):3. [PubMed: 21798081]

Dobrowolny G, Aucello M, Rizzuto E, Beccafico S, Mammucari C, Boncompagni S, Belia S, Wannenes F, Nicoletti C, Del Prete Z, Rosenthal N, Molinaro M, Protasi F, Fano G, Sandri M, Musaro A. Skeletal muscle is a primary target of SOD1G93A-mediated toxicity. Cell Metab. 2008; 8:425–436. [PubMed: 19046573]

Dupuis L, Gonzalez De Aguilar JL, Echaniz-Laguna A, Loeffler JP. Mitochondrial dysfunction in amyotrophic lateral sclerosis also affects skeletal muscle. Muscle Nerve. 2006; 34:253–254. [PubMed: 16642501]

Ferreira R, Bernardino L. Dual role of microglia in health and disease: pushing the balance toward repair. Front Cell Neurosci. 2015; 9:51. [PubMed: 25745386]

Feske S, Wulff H, Skolnik EY. Ion channels in innate and adaptive immunity. Annu. Rev. Immunol. 2015; 33:291–353. [PubMed: 25861976]

Fiala M, Chattopadhay M, La Cava A, Tse E, Liu G, Lourenco E, Eskin A, Liu PT, Magpantay L, Tse S, Mahanian M, Weitzman R, Tong J, Nguyen C, Cho T, Koo P, Sayre J, Martinez-Maza O, Rosenthal MJ, Wiedau-Pazos M. IL-17 is increased in the serum and in spinal cord CD8 and mast cells af ALS patient. J Neuroinflammation. 2010; 7:76. [PubMed: 21062492]

Fioretti B, Catacuzzeno L, Sforna L, Aiello F, Pagani F, Ragozzino D, Castigli E, Franciolini F. Histamine hyperpolarizes human glioblastoma cells by activating the intermediate-conductance Ca2+-activated K+ channel. Am J Physiol Cell Physiol. 2009; 297(1):C102–10. [PubMed: 19420000]

Fischer LR, Culver DG, Tennant P, Davis AA, Wang M, Castellano-Sanchez A, Khan J, Polak MA, Glass JD. Amyotrophic lateral sclerosis is a distal axonopathy: evidence in mice and man. Exp Neurol. 2004; 185:232–40. [PubMed: 14736504]

Fischer-Hayes LR, Brotherton T, Glass JD. Axonal degeneration in the peripheral nervous system: Implications for the pathogenesis of amyotrophic lateral sclerosis. Exp Neurol. 2013; 246:6–13. [PubMed: 23664960]

Frakes AE, Ferraiuolo L, Haidet-Phillips AM, Schmelzer L, Braun L, Miranda CJ, Ladner KJ, Bevan AK, Foust KD, Godbout JP, Popovich PG, Guttridge DC, Kaspar BK. Microglia induce motor neuron death via the classical NF-kappaB pathway in amyotrophic lateral sclerosis. Neuron. 2014; 81(5):1009–23. [PubMed: 24607225]

Grimaldi A, D'Alessandro G, Golia MT, Grössinger EM, Di Angelantonio S, Ragozzino D, Santoro A, Esposito V, Wulff H, Catalano M, Limatola C. KCa3.1 inhibition switches the phenotype of glioma-infiltrating microglia/macrophages. Cell Death Dis. 2016; 7:e2174. [PubMed: 27054329]

Hall ED, Oostveen JA, Gurney ME. Relationship of microglial and astrocytic activation to disease onset and progression in a transgenic model of familial ALS. Glia. 1998; 23:249–256. [PubMed: 9633809]

Henkel JS, Engelhardt JI, Siklós L, Simpson EP, Kim SH, Pan T, Goodman JC, Siddique T, Beers DR, Appel SH. Presence of dendritic cells, MCP-1, and activated microglia/macrophages in amyotrophic lateral sclerosis spinal cord tissue. Ann Neurol. 2004; 55:221–235. [PubMed: 14755726]

Kaushal V, Koeberle PD, Wang Y, Schlichter LC. The Ca2+-activated K+ channel KCNN4/KCa3.1 contributes to microglia activation and nitric oxide-dependent neurodegeneration. J Neurosci. 2007; 27:234–244. [PubMed: 17202491]

Kilkenny C, Browne WJ, Cuthill IC, Emerson M, Altman DG. Improving bioscience research reporting: the ARRIVE guidelines for reporting animal research. PLoS Biol. 2010; 8(6):e1000412. [PubMed: 20613859]

Kim HY, Kim H, Oh KW, Oh SI, Koh SH, Baik W, Noh MY, Kim KS, Kim SH. Biological markers of mesenchymal stromal cells as predictors of response to autologous stem cell transplantation in patients with amyotrophic lateral sclerosis: an investigator-initiated trial and in vivo study. Stem Cells. 2014; 32(10):2724–31. [PubMed: 24966156]

Koizumi S, Shigemoto-Mogami Y, Nasu-Tada K, Shinozaki Y, Ohsawa K, Tsuda M, Joshi BV, Jacobson KA, Kohsaka S, Inoue K. UDP acting at P2Y6 receptors is a mediator of microglial phagocytosis. Nature. 2007; 446:1091–1095. [PubMed: 17410128]

Krasnianski A, Deschauer M, Neudecker S, Gellerich FN, Müller T, Schoser BG, Krasnianski M, Zierz S. Mitochondrial changes in skeletal muscle in amyotrophic lateral sclerosis and other neurogenic atrophies. Brain. 2005; 128:1870–1876. [PubMed: 15901649]

Lee J, Park J, Kim S, Park I, Seo YS. Differential regulation of neuronal and inducible nitric oxide synthase (NOS) in the spinal cord of mutant SOD1 (G93A) ALS mice. Biochem Biophys Res Commun. 2016; 387(1):202–6.

Léger B, Vergani L, Sorarù G, Hespel P, Derave W, Gobelet C, D'Ascenzio C, Angelini C, Russell AP. Human skeletal muscle atrophy in amyotrophic lateral sclerosis reveals a reduction in Akt and an increase in atrogin-1. FASEB J. 2006; 20:583–585. [PubMed: 16507768]

Lewis KE, Rasmussen AL, Bennett W, King A, West AK, Chung RS, Chuah MI. Microglia and motor neurons during disease progression in the SOD1G93A mouse model of amyotrophic lateral sclerosis: changes in arginase1 and inducible nitric oxide synthase. J Neuroinfl. 2014; 11:55.

Liao B, Zhao W, Beers DR, Henkel JS, Appel SH. Transformation from a neuroprotective to a neurotoxic microglial phenotype in a mouse model of ALS. Exp Neurol. 2012; 237:147–152. [PubMed: 22735487]

Lu CH, Allen K, Oei F, Leoni E, Kuhle J, Tree T, Fratta P, Sharma N, Sidle K, Howard R, Orrell R, Fish M, Greensmith L, Pearce N, Gallo V, Malaspina A. Systemic inflammatory response and neuromuscular involvement in amyotrophic lateral sclerosis. Neurol Neuroimmunol Neuroinfl. 2016; 3(4):e244.

Ludolph AC, Bendotti C, Blaugrund E, Hengerer B, Löffler JP, Martin J, Meininger V, Meyer T, Moussaoui S, Robberecht W, Scott S, Silani V, Van Den Berg LH. ENMC Group for the Establishment of Guidelines for the Conduct of Preclinical and Proof of Concept Studies in ALS/MND Models. Guidelines for preclinical animal research in ALS/MND: a consensus meeting. Amyotroph. Lateral Scler. 2010; 11:38–45. [PubMed: 20184514]

Maezawa I, Jenkins DP, Jin BE, Wulff H. Microglial KCa3.1 channels as a potential therapeutic target for Alzheimer's disease. Int J Alzheimer Dis. 2012:868972.

Maezawa I, Zimin PI, Wulff H, Jin LW. Amyloid-beta protein oligomer at low nanomolar concentrations activates microglia and induces microglial neurotoxicity. J Biol Chem. 2011; 286:3693–3706. 2011. [PubMed: 20971854]

Mantovani S, Garbelli S, Pasini A, Alimonti D, Perotti C, Melazzini M, Bendotti C, Mora G. Immune system alterations in sporadic amyotrophic lateral sclerosis patients suggest an ongoing neuroinflammatory process. J Neuroimmunol. 2009; 210:73–79. [PubMed: 19307024]

Manzano R, Toivonen JM, Oliván S, Calvo AC, Moreno-Igoa M, Muñoz MJ, Zaragoza P, García-Redondo A, Osta R. Altered expression of myogenic regulatory factors in the mouse model of amyotrophic lateral sclerosis. Neurodegener Dis. 2011; 8:386–396. [PubMed: 21346327]

Martinou JC, Merlie JP. Nerve-dependent of acetylcholine receptor epsilon-subunit gene expression. J. Neurosci. 1991; 11:1291–1299. [PubMed: 2027048]

Moloney EB, de Winter F, Verhaagen J. ALS as a distal axonopathy: molecular mechanisms affecting neuromuscular junction stability in the presymptomatic stages of the disease. Front Neurosci. 2014; 8:252. [PubMed: 25177267]

Morrison HW, Filosa JA. A quantitative spatiotemporal analysis of microglia morphology during ischemic stroke and reperfusion. J Neuroinfl. 2013; 10:1–20.

Nguyen HM, Grössinger EM, Horiuchi M, Davis KW, Jin LW, Maezawa I, Wulff H. Differential Kv1.3, KCa3.1, and Kir2.1 expression in "classically" and "alternatively" activated microglia. Glia. 2017; 65:106–121. [PubMed: 27696527]

Ohsawa K, Irino Y, Sanagi T, Nakamura Y, Suzuki E, Inoue K, Kohsaka S. P2Y12 receptor-mediated integrinβ1 activation regulates microglial process extension induced by ATP. Glia. 2010; 58:790–801. [PubMed: 20091784]

Paolicelli RC, Jawaid A, Henstridge CM, Valeri A, Merlini M, Robinson JL, Rose J, Appel S, Lee VM, Trojanowski JQ, Spires-Jones T, Schulz PE, Rajendran L. TDP-43 Depletion in Microglia Promotes Amyloid Clearance but Also Induces Synapse Loss. Neuron. 2017; 95(2):297–308. e6. [PubMed: 28669544]

Pasetto L, Pozzi S, Castelnovo M, Basso M, Estevez AG, Fumagalli S, De Simoni MG, Castellaneta V, Bigini P, Restelli E, Chiesa R, Trojsi F, Monsurrò MR, Callea L, Malešević M, Fischer G, Freschi M, Tortarolo M, Bendotti C, Bonetto V. Targeting Extracellular CyclophilinA Reduces Neuroinflammation and Extends Survival in a Mouse Model of Amyotrophic Lateral Sclerosis. J Neurosci. 8. 2017; 37(6):1413–1427.

Philips T, Robberecht W. Neuroinflammation in amyotrophic lateral sclerosis: role of glial activation in motor neuron disease. Lancet Neurol. 2011; 10:253–263. [PubMed: 21349440]

Phul RK, Shaw PJ, Ince PG, Smith ME. Expression of nitric oxide synthase isoforms in spinal cord in amyotrophic lateral sclerosis. Amyotroph Lateral Scler Other Motor Neuron Disord. 2000; 1:259–267. [PubMed: 11465019]

Puentes F, Malaspina A, van Noort JM, Amor S. Non-neuronal cells in ALS: role of glial, immune cells and blood-CNS barriers. Brain Pathol. 2016; 26:248–257. [PubMed: 26780491]

Reich E, Cui L, Yang L, Pugliese-Sivo C, Golovko A, Petro M, Vassileva G, Chu I, Nomeir AA, Zhang LK, Liang X, Kozlowski JA, Narula SK, Zavodny PJ, Chou CC. Blocking ion channel KCNN4 alleviates the symptoms of experimental autoimmune encephalomyelitis in mice. Eur. J. Immunol. 2005; 35:1027–1036. [PubMed: 15770697]

Rinaldi A, Defterali C, Mialot A, Garden DL, Beraneck M, Nolan MF. HCN1 channels in cerebellar Purkinje cells promote late stages of learning and constrain synaptic inhibition. J. Physiol. 2013; 591:5691–5709. [PubMed: 24000178]

Robberecht W, Philips T. The changing scene of amyotrophic lateral sclerosis. Nat. Rev. Neurosci. 2013; 14:248–264. [PubMed: 23463272]

Rothstein JD. Current hypotheses for the underlying biology of amyotrophic lateral sclerosis. Ann. Neurol. 2009; 65(Suppl 1):S3–S9. [PubMed: 19191304]

Shruthi S, Sumitha R, Varghese AM, Ashok S, ChandrasekharSagar BK, Sathyaprabha TN, Nalini A, Kramer BW, Raju TR, Vijayalakshmi K, Alladi PA. Brain-Derived Neurotrophic Factor Facilitates Functional Recovery from ALS-Cerebral Spinal Fluid-Induced Neurodegenerative Changes in the NSC-34 Motor Neuron Cell Line. Neurodegener. Dis. 2017; 17(1):44–58. [PubMed: 27617773]

Stowe DF, Aldakkak M, Camara AK, Riess ML, Heinen A, Varadarajan SG, Jiang MT. Cardiac mitochondrial preconditioning by big Ca2+- sensitive K+ channel opening requires superoxide radical generation. Am J Physiol Heart Circ Physiol. 2006; 290:H434–H440. [PubMed: 16126810]

Tanaka K, Kanno T, Yanagisawa Y, Yasutake K, Hadano S, Yoshii F, Ikeda JE. Bromocriptine methylate suppresses glial inflammation and moderates disease progression in a mouse model of amyotrophic lateral sclerosis. Exp Neurol. 2011; 232(1):41–52. [PubMed: 21867702]

Toyama K, Wulff H, Chandy KG, Azam P, Raman G, Saito T, Fujiwara Y, Mattson DL, Das S, Melvin JE, Pratt PF, Hatoum OA, Gutterman DD, Harder DR, Miura H. The intermediate-conductance calcium-activated potassium channel KCa3.1 contributes to atherogenesis in mice and humans. J Clin Invest. 2008; 118:3025–3037. [PubMed: 18688283]

Turner MR, Cagnin A, Turkheimer FE, Miller CC, Shaw CE, Brooks DJ, Leigh PN, Banati RB. Evidence of widespread cerebral microglial activation in amyotrophic lateral sclerosis: an [11C] (R)-PK11195 positron emission tomography study. Neurobiol Dis. 2004; 15(3):601–9. [PubMed: 15056468]

Vallarola A, Sironi F, Tortarolo M, Gatto N, De Gioia R, Pasetto L, De Paola M, Mariani A, Ghosh S, Watson R, Kalmes A, Bonetto V, Bendotti C. RNS60 exerts therapeutic effects in the SOD1 ALS mouse model through protective glia and peripheral nerve rescue. J Neuroinflammation. 2018; 15(1):65. [PubMed: 29495962]

Wulff H, Miller Mark J, Hänsel Wolfram, Grissmer Stephan, Cahalan Michael D, Chandy K George. Design of a potent and selective inhibitor of the intermediate-conductance Ca2+-activated K+ channel, IKCa1: a potential immunosuppressant. Proc Natl Acad Sci. 2000; 97:8151–8156. [PubMed: 10884437]

Ye J, Jiang Z, Chen X, Liu M, Li J, Liu N. Electron transport chain inhibitors induce microglia activation through enhancing mitochondrial reactive oxygen species production. Exp Cell Res. 2016; 340(2):315–26. [PubMed: 26511505]

Yip PK, Kaan TK, Fenesan D, Malcangio M. Rapid isolation and culture of primary microglia from adult mouse spinal cord. J Neurosci Methods. 2009; 183(2):223–37. [PubMed: 19596375]

Zierler S, Sumoza-Toledo A, Suzuki S, Dúill FÓ, Ryazanova LV, Penner R, Ryazanov AG, Fleig A. TRPM7 kinase activity regulates murine mast cell degranulation. J Physiol. 2016; 594(11):2957–70. [PubMed: 26660477]

- *kcnn4* is overexpressed in spinal microglia from symptomatic hSOD1^{G93A} mice
- the inhibition of KCa3.1 shifts hSOD1^{G93A} microglia to anti-inflammatory phenotype
- the inhibition of KCa3.1 delays disease onset in hSOD1^{G93A} mice
- the inhibition of KCa3.1 preserves NMJ junction functionality in hSOD1^{G93A} mice

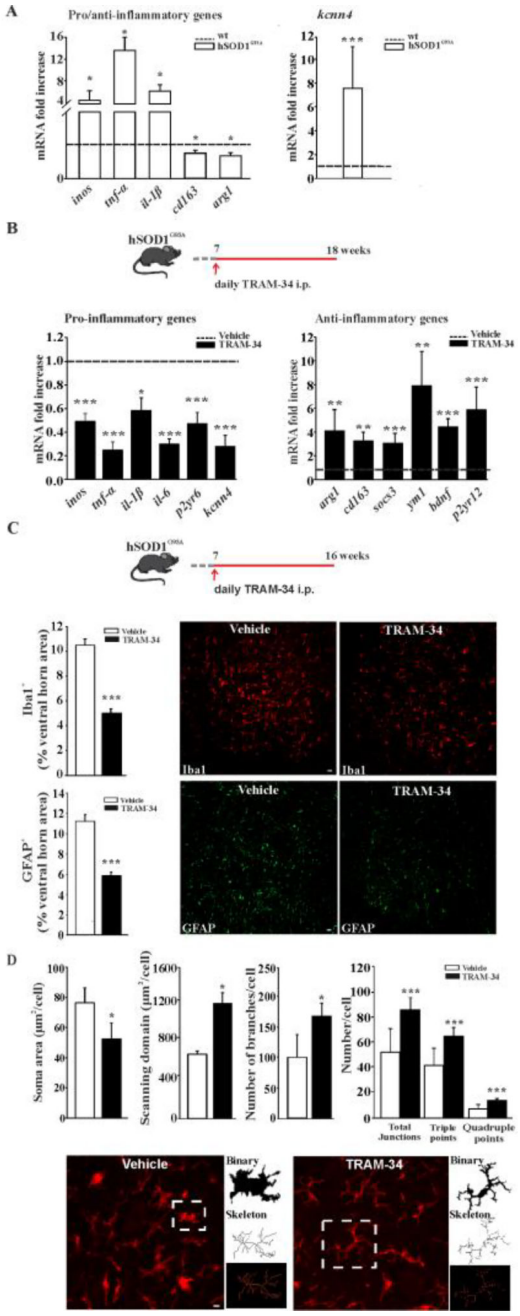

Figure 1. KCa3.1 channels shape microglia activation in ALS

A: Relative expression level of *inos, tnf-α, il-1β, cd163 and arg1* (left) and *kcnn4* (right) in microglial cells isolated from 18 week-old hSOD1^{G93A} mice compared to each gene in *wt* mice (dotted line) (data are shown as mean ± SEM, n=3, * < 0.05, *** p<0.001 *vs wt*, Student's *t* test). **B:** top, treatment scheme. RT-PCR analyses of the relative expression level of pro- **(left)** and anti- **(right)** inflammatory and *kcnn4* genes in microglia cells isolated from the lumbar region of the spinal cord of hSOD1^{G93A} mice expressed as fold increase of TRAM-34-treated *vs* vehicle treated mice (dotted line); data are shown as mean fold increase ± SEM; *p<0.05, ** p<0.01, *** p<0.001 *vs* vehicle by Student's t-test n= 6, **C:**

top, treatment scheme. Quantification of Iba1$^+$ (**upper panel**) and GFAP$^+$ (**lower panel**) staining in the lumbar region of the spinal cord of vehicle (white bar) and TRAM-34 treated (black bar) mice (data are shown as mean ± SEM. *** p<0.001 *vs* vehicle by Student's t test, n=5 vehicle, n=6 TRAM-34). Representative immunofluorescence images are shown on the right (scale bar=20μm). **D:** Morphological analysis of lumbar Iba1$^+$ cells: from left, soma area (TRAM-34 50.92 ± 10.36 μm^2 *vs* vehicle 74.23 ± 9.59 μm^2 *p<0.002), scanning domain (TRAM-34 1221.75 ± 113.68 μm *vs* vehicle 683.20 ± 35.27 μm *p<0.010), number of branches per cell (TRAM-34 167.88 ± 21.56 *vs* vehicle 100.50 ± 37.19 ***p<0.001), junctions (total, 85.56 ± 10.67 *vs* 52.03 ± 18.80; triple, 64.71 ± 7.34 *vs* 41.62 ± 13.66; quadruple 14.02 ± 2.24 *vs* 7.29 ± 3.63 ***p<0.001) (data are shown as mean ± SEM, 20 cells, 6 slices, 4 mice per condition, by Student's t-test). Bottom: representative images of maximum intensity projections of a confocal z-stack imaging of Iba1$^+$ cells, converted to binary images and then skeletonized (scale bar=20μm).

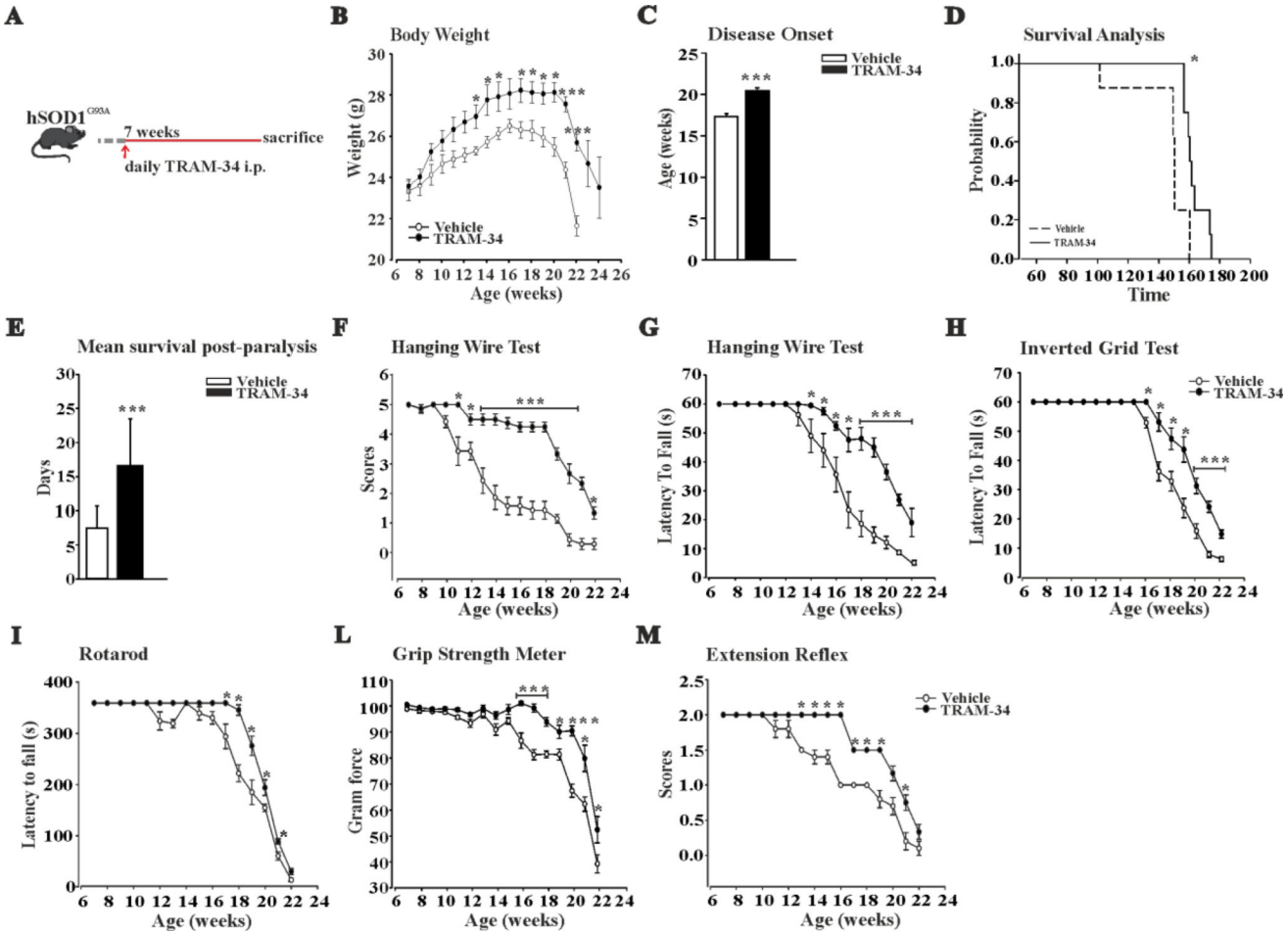

Figure 2. KCa3.1 channels modulate motor function and survival in hSOD1^{G93A} mice

A: Treatment scheme. **B:** Variations of body weight over time in vehicle (white) and TRAM-34-treated hSOD1G93A mice (black dots). Data are the mean ± SEM; *p<0.05, ** p<0.01, *** p<0.001 *vs* vehicle by Student's t-test n= 9. **C:** Disease onset index, calculated as the age of peak of body weight. Disease onset in TRAM-34 treated mice was 19.3 ± 0.2 weeks, black bars; in vehicle 16.3 ± 0.2 weeks, white bars. Data are the mean ± SEM *** p<0.001, n=9. **D:** Kaplan–Meier analysis of mice survival. TRAM-34 increased the survival time of hSOD1^{G93A} mice (TRAM-34: 165 ± 2 days; vehicle: 148 ± 7 days, data are the mean ± SEM *p<0.008 by Log–rank test, n=9). **E:** Quantification of the mean survival time post-paralysis. TRAM-34: 16.6 ± 2.41 days (black bar); vehicle: 7.4 ± 0.97 days (white bar) data are the mean ± SEM, n=9 ***p<0.001 by Student's t test. **F–M:** Analyses of motor function in SOD1^{G93A} mice treated with TRAM-34 (black dots) or vehicle (white dots) with: hanging wire test, score (**F**) and latency (**G**), inverted grid test (**H**), rotarod test (**I**), grip strength test (force) (**L**) and extension reflex (**M**). Behavioral tests were performed once a week, starting from 7-weeks of age until weeks described in the panels. All behavioral tests were ameliorated by TRAM-34 treatment. Data are expressed as mean ± SEM; *p<0.05, ** p<0.01, *** p<0.001 *vs* vehicle hSOD1^{G93A} mice by Student's t-test n= 9.

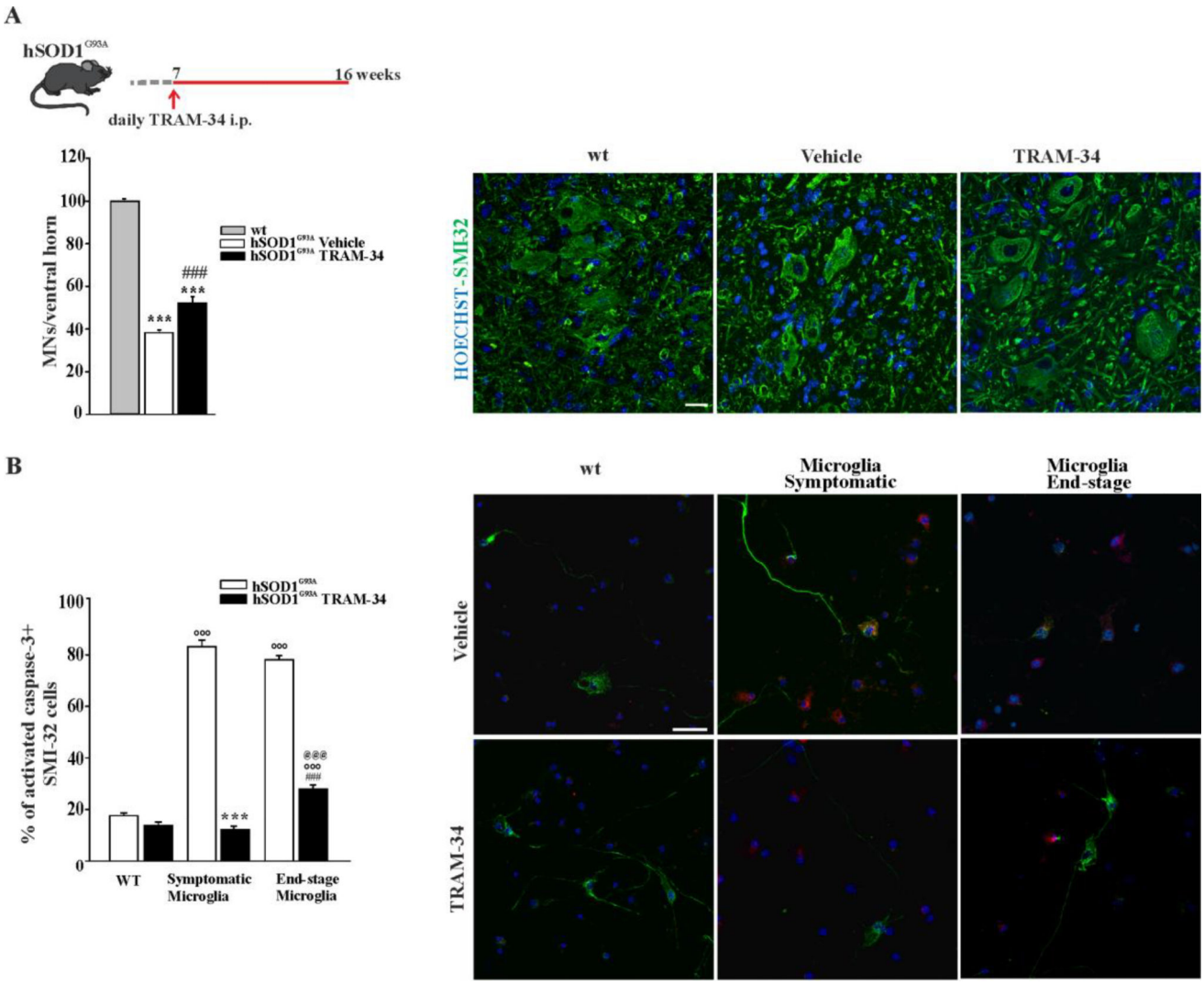

Figure 3. KCa3.1 channels modulate microglia-motor neuron interaction in hSOD1^{G93A} mice

A: top, treatment scheme. Bottom, quantification of MNs (counted as SMI-32 stained cells in the ventral horns of the spinal cord) in non-tg *wt*, and hSOD1^{G93A} mice treated with vehicle or TRAM-34. Data are shown as mean ± SEM ***p<0.001 *vs wt;* ###p<0.001 *vs* vehicle by One Way ANOVA, TRAM-34 n=6; Vehicle n=5; *wt* n=3). Representative immunofluorescence images are shown on the right (scale bar=20μm). **B** Non-tg *wt* MNs co-cultured with microglia isolated from the spinal cord of *wt*, symptomatic or end-stage hSOD1^{G93A} mice treated with TRAM-34 (2.5 μM, black bars) or DMSO (white bars). After 72 h, MN death was quantified counting the activated caspase 3/SMI32 double positive cells. Data are mean ± SEM; n=3 in triplicate, °°°p<0.001 *vs wt* microglia, ***p<0.001 vs symptomatic microglia, ###p<0.001 vs end-stage microglia, @@@p<0.001 vs *wt* microglia +TRAM-34 by Two Way ANOVA (Holm-Sidak method): Representative immunofluorescence images are shown on the right (scale bar=20μm).

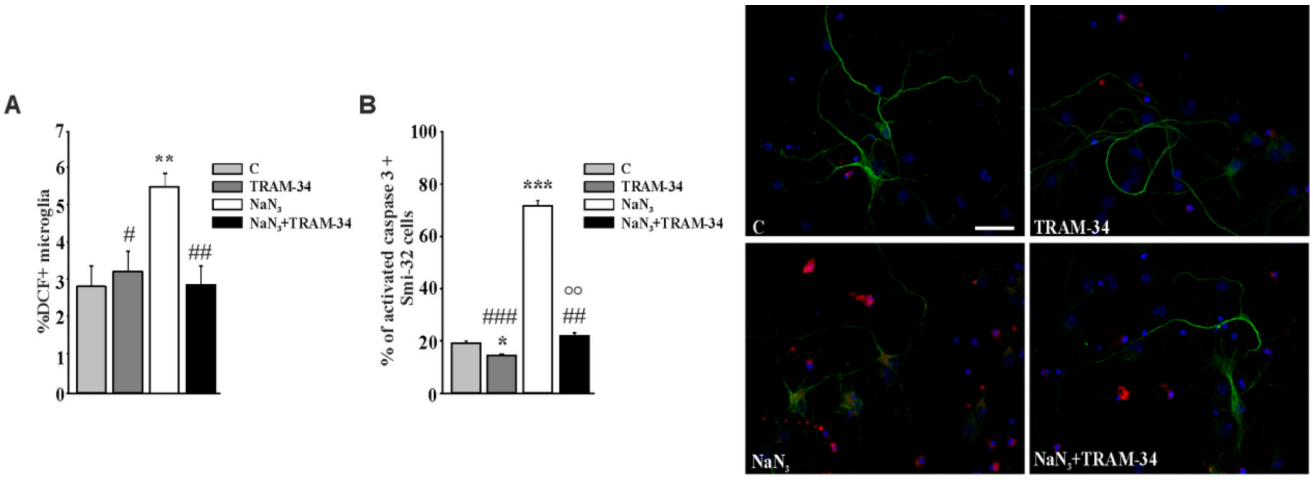

Figure 4. MNs are protected against ROS neurotoxicity by TRAM-34 treated microglia

A: Quantification of ROS production in non-tg *wt* microglia treated with NaN_3 (5μM), vehicle (DMSO, control) or TRAM-34 (2.5 μM) for 18 h, measured as dichlorofluorescein positive cells by cytofluorimetry (Data are expressed as % of DCF^+ microglia, mean ± SEM, n=3 in triplicate, **p=0.005 vs C; #p=0.048, ##p=0.004 vs NaN_3 by Two Way ANOVA (Holm-Sidak method). **B:** Cell death quantification of MNs co-cultured for 24h with non-tg wt microglia pre-treated as in **A**. Data are expressed as % of active-caspase 3/SMI32 double positive cells on SMI32 positive cells in each condition and are the mean ± SEM. n=3 in triplicate, ***p<0.001, *p=0.037 v*s* control, ## p=0.003, ### p<0.001 vs NaN_3, °°p=0.003 vs TRAM-34 by Two Way ANOVA (Holm-Sidak method). Representative immunofluorescence images are shown on the right (scale bar=20μm).

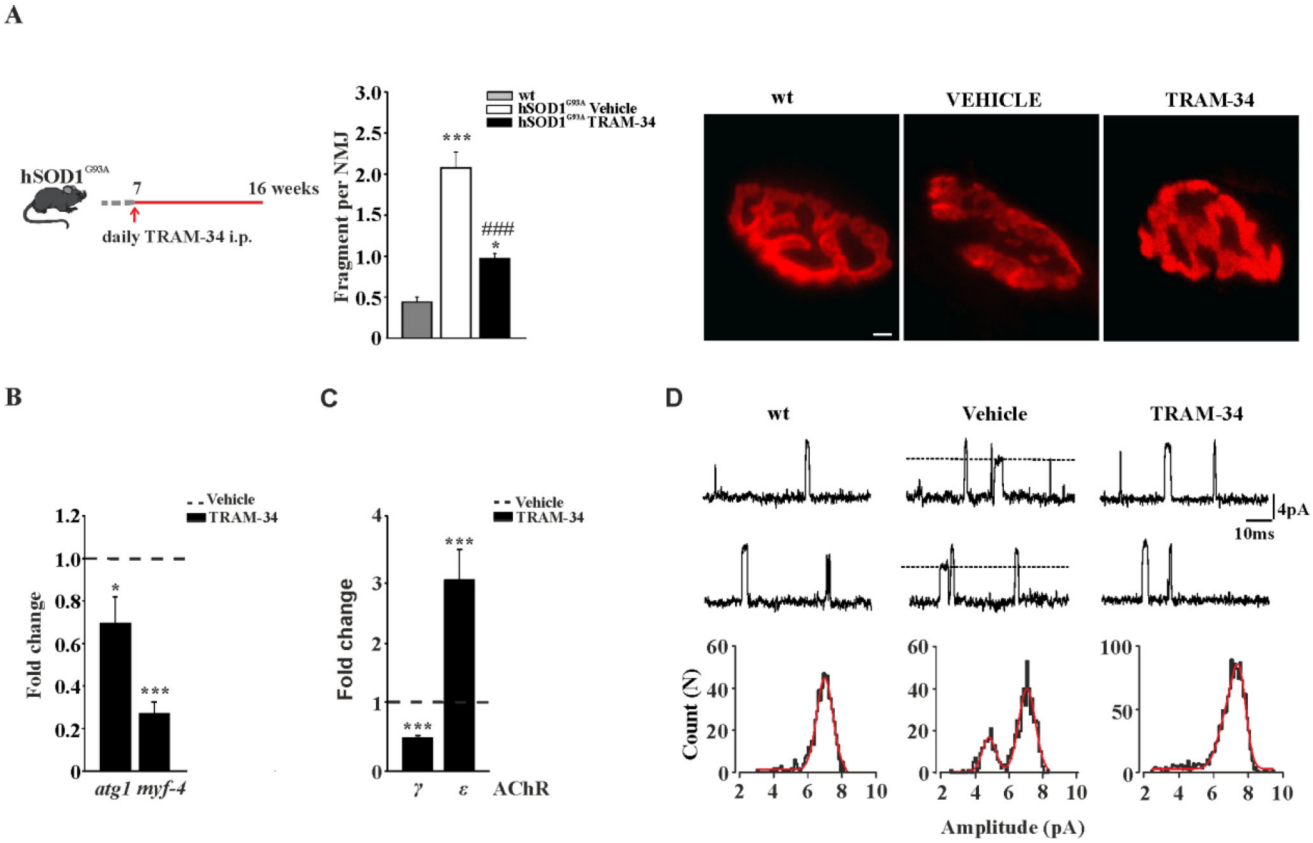

Figure 5. KCa3.1 channel inhibition ameliorates NMJs functionality

A: left, treatment scheme. Center, AChR fragments per NMJ in the different conditions, as indicated (mean ± SEM, n = 4 mice; *p<0.05, ***p<0.001 vs *wt*, ###p<0.001 vs vehicle; 130 α-BTX-positive NMJ per group were randomly chosen and analyzed). Right, representative images of *tibialis anterior* (TA) muscles stained with α-BTX for each experimental group (scale bar=20μm). **B:** Relative expression of *atg1* and *myf4* in the TA muscle of 16-weeks old mice. Data are normalized to GAPDH and expressed as fold changes ± SEM vs vehicle treated hSOD1^{G93A} mice (n=3–4). **C:** Relative expression of γ and ε AChR in TA muscles from vehicle and TRAM-34-treated hSOD1^{G93A} mice. Data are normalized to GAPDH and expressed as fold changes ± SEM *vs* vehicle. **D:** Single channel recordings of (ACh)-evoked unitary events in *FDB* muscle fibres dissociated from non-tg, vehicle and TRAM-34 treated hSOD1^{G93A} mice. In the top and middle, non-consecutive traces recorded in an end-plate evoked by ACh (200 μM) at an estimated patch potential of −85mV. Dotted lines indicate openings of ACh-γ found only in vehicle hSOD1^{G93A} mice. Lower, histograms of the of unitary events, best fitted by two Gaussian functions (continuous line) only in the vehicle hSOD1^{G93A} group.